Acta Crystallographica Section D
Biological Crystallography
ISSN 0907-4449

Nonlinear temperature dependence of the crystal structure of lysozyme: correlation between coordinate shifts and thermal factors

Yasumasa Joti,[a,b] Masayoshi Nakasako,[c] Akinori Kidera[b]* and Nobuhiro Go[a]

[a]Department of Science, Kyoto University, Kitashirakawa, Sakyo-ku, Kyoto 606-8502, Japan, [b]Department of Integrated Science, Yokohama City University, 1-7-29 Suehirocho, Tsurumi-ku, Yokohama 230-0045, Japan, and [c]Department of Physics, Faculty of Science and Engineering, Keio University and PRESTO, Japan Science and Technology Corporation, 3-14-1 Hiyoshi, Kohoku-ku, Yokohama, Kanagawa 223-8522, Japan

Correspondence e-mail: kidera@tsurumi.yokohama-cu.ac.jp

Received 31 January 2002
Accepted 24 June 2002

PDB References: lysozyme, 113 K, 1iwt, r1iwtsf; 127 K, 1iwu, r1iwusf; 147 K, 1iwv, r1iwvsf; 152 K, 1iww, r1iwwsf; 161 K, 1iwx, r1iwxsf; 170 K, 1iwy, r1iwysf; 178 K, 1iwz, r1iwzsf.

The static and dynamic structures of human lysozyme at seven different temperatures ranging from 113 to 178 K were investigated by normal-mode refinement of the cryogenic X-ray diffraction data collected from a single crystal. Normal-mode refinement decomposes the mean-square fluctuations of protein atoms from their average position into the contributions from the internal degrees of freedom, which change the shape of the protein structure, and those from the external degrees of freedom, which generate rigid-body motions in the crystal. While at temperatures below 150 K the temperature dependence of the total mean-square fluctuations shows a small gradient similar to that predicted theoretically by normal-mode analysis, at temperatures above 150 K there is an apparent inflection in the temperature dependence with a higher gradient. The inflection in the temperature dependence at temperatures above 150 K occurs mostly in the external degrees of freedom. Possible causes for the dynamic transition are discussed with respect to the crystal packing and physicochemical properties of crystalline water.

1. Introduction

Crystallographic thermal factors (or Debye–Waller factors) of protein molecules provide a wealth of information about protein dynamics. Atomically detailed features of thermal factors can potentially provide valuable information about protein function (Frauenfelder, 1989). Since the pioneering work by Frauenfelder *et al.* (1979), the mean-square fluctuations around the average position, $\langle \Delta r^2 \rangle_{\rm total}$, derived from the thermal factors of protein atoms have often been discussed with respect to their temperature dependence (Hartmann *et al.*, 1982; Parak *et al.*, 1987; Tilton *et al.*, 1992; Kurinov & Harrison, 1995; Nagata *et al.*, 1996).

Rasmussen *et al.* (1992) observed that crystalline ribonuclease A (RNase A) lost its binding activity to an inhibitor at ~220 K. They claimed that, at the same temperature, there was an inflection in the temperature dependence of $\langle \Delta r^2 \rangle_{\rm total}$. It has been argued that this inflection is a result of a glass transition in the protein dynamics from harmonic to anharmonic diffusive motions observed in various spectroscopic measurements using, for example, Mössbauer spectroscopy (Parak *et al.*, 1982), Rayleigh scattering of Mössbauer radiation (Nienhaus & Parak, 1986) and neutron incoherent scattering (Doster *et al.*, 1989; Ferrand *et al.*, 1993). The correspondence between the dynamic transition and the onset of the activity leads to a hypothesis that the substrate-binding activity of RNase A requires diffusive anharmonic motions

acquired above the transition temperature. However, in our previous study, crystalline myoglobin showed no clear inflection in the temperature dependence of $\langle \Delta r^2 \rangle_{\rm total}$ at temperatures between 40 and 300 K (Chong *et al.*, 2001). Moreover, even after $\langle \Delta r^2 \rangle_{\rm total}$ had been decomposed into contributions from the internal degrees of freedom, $\langle \Delta r^2 \rangle_{\rm int}$, and those from the external degrees of freedom, $\langle \Delta r^2 \rangle_{\rm ext}$, by the normal-mode refinement (Kidera & Go, 1992; Joti & Kidera, in preparation),

$$\langle \Delta r^2 \rangle_{\rm total} = \langle \Delta r^2 \rangle_{\rm int} + \langle \Delta r^2 \rangle_{\rm ext}, \qquad (1)$$

the temperature dependence of both $\langle \Delta r^2 \rangle_{\rm int}$ and $\langle \Delta r^2 \rangle_{\rm ext}$ exhibited no inflection in the gradient at ~200 K. These crystallographic studies on RNase A and myoglobin do not necessarily contradict each other. It should be noted that both proteins undergo a dynamic transition at ~200 K, as was observed in binding-affinity experiments on RNase A (Hagen *et al.*, 1995) and spectroscopic studies of myoglobin (Parak *et al.*, 1982; Doster *et al.*, 1989). However, as discussed by Chong *et al.* (2001), because of the coherent nature of X-ray diffraction, $\langle \Delta r^2 \rangle_{\rm total}$ determined from crystallographic thermal factors represents static distribution, which is totally different from the value of $\langle \Delta r^2 \rangle_{\rm total}$ determined in the incoherent spectroscopic experiments measuring the time correlation. Therefore, if the same set of conformational substates is occupied throughout the temperature range being examined, the dynamic transition cannot be observed in X-ray diffraction, but is observed in the incoherent experiments, as schematically illustrated in Fig. 1(*a*). In this sense, the linear temperature dependence of $\langle \Delta r^2 \rangle_{\rm int}$ in myoglobin means that all the substates are occupied at all the temperatures. On the other hand, if a certain substate becomes vacant at a low temperature, the dynamic transition may be observed even in X-ray diffraction (Fig. 1*b*). This may correspond to the results in RNase A (Rasmussen *et al.*, 1992; Tilton *et al.*, 1992). It is noted that when dynamic transition is observed in X-ray diffraction, abrupt changes in the average positions should simultaneously occur at the same transition temperature, as schematically illustrated in Fig. 1(*b*). Another possibility in the transition described in Fig. 1(*c*) was found in this study and will be discussed later.

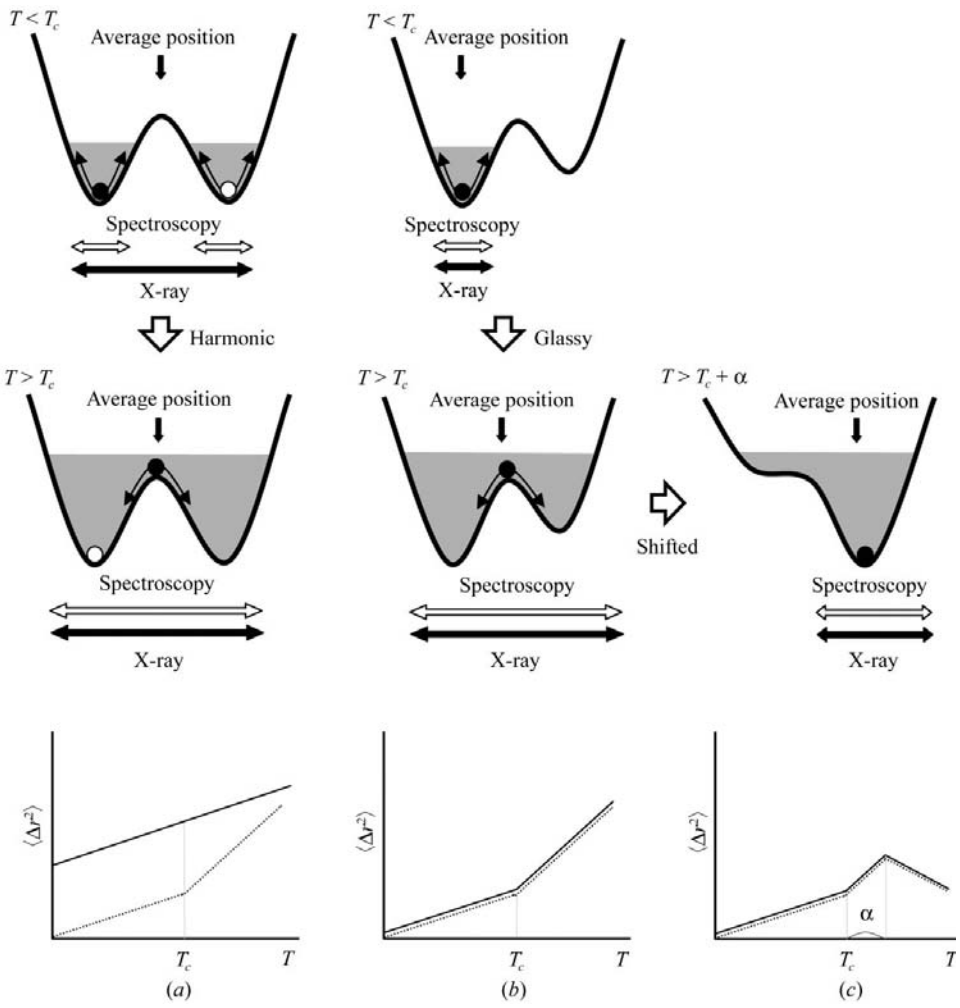

Figure 1
A schematic explanation of the temperature dependence of the Debye–Waller factors observed in X-ray diffraction (solid line) and incoherent spectroscopy (dotted line). (*a*) When all the conformational substates are occupied throughout all the temperature range, a glass transition is not observed in X-ray diffraction but is observed in incoherent experiments. We call this dynamic response 'harmonic' based on the nature of X-ray diffraction. (*b*) When a certain substate is not occupied at low temperatures but is occupied at high temperatures, dynamic transition may be observed even in X-ray diffraction experiments. Here, this dynamic response is called 'glassy'. (*c*) When the temperature is further increased after 'glassy' transition, we observe large coordinate shifts at some loci that diminish the population in the original position at low temperatures. In this case, the mean-square fluctuations decrease again after the 'glassy' transition. This dynamic response is different from those of the former two types and is called 'shifted'.

However, in the temperature dependence of $\langle \Delta r^2 \rangle_{\rm total}$ of RNase A (Rasmussen *et al.*, 1992; Tilton *et al.*, 1992), the inflection is actually too subtle to claim that this corresponds to the case illustrated in Fig. 1(*b*). One reason for this is that the diffraction data were collected from different crystals at different temperatures. In this paper, we present the results of normal-mode refinement of crystalline human lysozyme (EC 3.2.1.17) at temperatures between 113 and 178 K obtained based on diffraction data collected from only one crystal to avoid possible artifacts arising from the use of many crystals. Here, we show that

Table 1
Statistics in the diffraction data and the refined models.

Temperature (K)	113	127	147	152	161	170	178
Data collection							
Lattice constants (Å)							
a (Å)	56.17 (1)	56.18 (1)	56.22 (1)	56.29 (2)	56.33 (2)	56.40 (4)	56.57 (4)
b	60.98 (2)	61.00 (2)	61.04 (2)	61.12 (2)	61.13 (2)	61.15 (3)	61.18 (5)
c	33.17 (1)	33.17 (2)	33.19 (1)	33.10 (1)	33.09 (2)	33.09 (3)	33.04 (4)
Resolution (Å)	40.00–1.35	40.00–1.35	40.00–1.35	40.00–1.35	40.00–1.35	40.00–1.35	40.00–1.48
Mosaic spread† (°)	0.42	0.42	0.41	0.42	0.43	0.45	0.56
No. of collected reflections	236759	234749	236842	359305	235472	214542	161023
No. of unique reflections	24725	24725	24634	24825	24754	24532	19123
Completeness (%)	96.0 (94.4/59.9)‡	96.0 (94.2/59.6)‡	95.9 (94.7/58.7)‡	96.2 (95.3/60.7)‡	95.9 (94.9/59.2)‡	94.8 (92.6/48.3)‡	96.5 (98.7)§
$R_{\rm merge}(I)$¶ (%)	4.6 (11.8)††	4.6 (11.9)††	4.6 (11.4)††	5.2 (17.2)††	5.0 (19.3)††	6.3 (26.5)††	5.8 (28.1)§
$I/\sigma(I)$	43.8 (8.3)††	44.7 (8.4)††	44.9 (8.3)††	47.1 (6.6)††	38.6 (4.9)††	30.8 (2.8)††	28.0 (3.0)§
$R_{\rm iso}(I)$‡‡ (%)		1.2	1.6	6.8	8.8	13.2	18.7
Refinement							
Resolution (Å)	8.00–1.40	8.00–1.40	8.00–1.40	8.00–1.40	8.00–1.40	8.00–1.40	8.00–1.48
No. of reflections used ($F > 2\sigma$)	22533	22515	22546	22549	22402	22096	18521
No. of non-H protein atoms	1029	1029	1029	1029	1029	1029	1029
No. of water molecules	307	307	307	307	225	225	196
No. of ions	3	3	3	3	3	3	3
Isotropic thermal factor refinement							
R factor§§ (%)	17.8	18.0	17.7	19.1	20.4	21.3	22.5
$R_{\rm free}$¶¶ (%)	21.4	20.6	21.8	24.3	26.4	27.1	29.4
R.m.s.d. from ideality							
Bond (Å)	0.011	0.011	0.012	0.012	0.011	0.011	0.014
Angle (°)	2.3	2.2	2.2	2.2	1.9	1.9	2.7
Normal-mode refinement							
R factor§§ (%)	15.8	16.0	16.0	16.8	18.7	19.4	20.4
$R_{\rm free}$¶¶ (%)	18.6	18.4	19.7	19.0	21.8	23.4	23.9
R.m.s.d. from ideality†††							
Bond (Å)	0.011	0.011	0.011	0.011	0.011	0.011	0.016
Angle (°)	1.3	1.3	1.3	1.3	1.3	1.3	1.6

† Mosaic spread includes the divergence of the incident X-ray beam of ∼0.2°. ‡ Values in parentheses are for the resolution shells 1.42–1.40/1.37–1.35 Å. § Values in parentheses are for the resolution shell 1.50–1.48 Å. ¶ $R_{\rm merge}(I) = \sum_h \sum_i |I_i(h) - \langle I(h)\rangle| / \sum_h \sum_i I_i(h) \times 100$ (%), where $I_i(h)$ is the intensity of the *i*th observation of reflection *h*. †† Values in parentheses are for the resolution shell 1.37–1.35 Å. ‡‡ $R_{\rm iso}(I) = \sum_h |I_T(h) - I_{113\rm K}(h)|^2 / \sum_h I_{113\rm K}(h)^2 \times 100$ (%), where $I_T(h)$ and $I_{113\rm K}(h)$ are the observed amplitudes of reflection *h* in the experiments at temperature *T* and 113 K, respectively. The value was calculated for the reflections to the resolution limit of the data at temperature *T*. §§ $R = \sum_h |F_{\rm calc}(h) - F_{\rm obs}(h)| / \sum_h F_{\rm obs}(h) \times 100$ (%), where $F_{\rm obs}(h)$ and $F_{\rm calc}(h)$ are the observed and calculated structure factors of reflection *h*, respectively. ¶¶ In the isotropic thermal factor refinement, 10% of the total reflections were set aside for cross-validation of the refined structure model (Brünger, 1992). In the normal-mode refinement, 5% were used for the validation. †††A modified version of the parameter set of Engh & Huber (1991) was used.

the temperature dependence of $\langle \Delta r^2 \rangle_{\rm total}$ has a clear inflection, which has so far not been observed in X-ray diffraction studies. We then describe the temperature dependence of the internal and external contributions of the mean-square fluctuations derived from the normal-mode refinement and the correlation between structural changes and the dynamic transition. Finally, we discuss possible reasons why such temperature dependence was observed in the lysozyme crystal but not in the myoglobin crystal.

2. Materials and methods

2.1. X-ray diffraction experiments

Human lysozyme was crystallized in the orthorhombic crystal form ($P2_12_12_1$) under the conditions described in Takano *et al.* (1995). Prior to flash-cooling with liquid ethane, the harvested crystal was embedded in mineral oil by carefully and completely removing the mother liquor surrounding the crystal using the tip of a crystal-mounting device (Hampton Research, USA). The ethane-cooled crystal was transferred onto a goniometer under liquid nitrogen. The dimensions of the crystal were 0.25 × 0.25 × 0.1 mm.

The diffraction data were collected using an oscillation method with an R-AXIS IV system (Rigaku, Tokyo, Japan). An Ultrax18 X-ray generator (Rigaku, Japan) operated at 45 kV and 90 mA and a double-mirror-focusing optics system (Rigaku, Japan) were used. Nickel-filtered Cu $K\alpha$ radiation was used; the crystal-to-detector distance was 68 mm. During the measurement, the crystal was exposed to a stream of cold nitrogen gas from a cooling device (Rigaku, Japan). Seven data sets were collected from a single crystal while varying the temperature of the cold nitrogen gas from 113 to 178 K (Table 1). The temperature of the gas stream was calibrated with a thermocouple set at the sample position prior to data collection. Measurements at higher temperatures were hindered by hexagonal ice formation at temperatures above ∼180 K that could have broken the crystal. Each data set, consisting of 140 frames, was collected in 1 d, with an oscillation of 1.3° and 10 min exposure. The indexing, integration and processing of the diffraction data were carried out using the programs *DENZO* and *SCALEPACK* (Otwinowski & Minor, 1997). The statistics of the collected data are shown in Table 1.

Preliminary crystallographic structure refinement under the assumption of isotropic thermal factors was carried out with

the program *X-PLOR* (Brünger, 1992) and model building was performed using *TURBO-FRODO* (Biographics, France). The initial models of human lysozyme were taken from the Protein Data Bank (PDB; Berman *et al.*, 2000) (PDB code 1rex; Muraki *et al.*, 1996). Rounds of refinement based on the ordinary refinement protocol were performed by using a set of restraint parameters (Engh & Huber, 1991). Hydration water molecules were assigned from difference Fourier $F_o - F_c$ maps using the program *FESTKOP* (Nakasako, 2001), taking the geometry of hydrogen bonds into account. The new parts of the model were examined using omit-annealed difference Fourier maps in the subsequent rounds of refinement. The final statistics of the preliminary refinement are shown in Table 1.

2.2. Normal-mode refinement

In the normal-mode refinement (Kidera & Go, 1992; Kidera *et al.*, 1992), the crystallographic structure factor F_c is represented by

$$\begin{aligned} F_c(\mathbf{q}) &= \sum_j f_j(\mathbf{q}) \exp(i\mathbf{q}\cdot\langle\mathbf{r}_j\rangle) \exp(-\tfrac{1}{2}\mathbf{q}^t\mathbf{U}_j\mathbf{q}) \\ &= \sum_j f_j(\mathbf{q}) \exp(i\mathbf{q}\cdot\langle\mathbf{r}_j\rangle) \\ &\quad \times \exp\Bigg[-\frac{1}{2}\sum_{s,t=1}^{3} q_s q_t \Bigg(\sum_{m,n=1}^{M} \varphi^I_{jsm}\varphi^I_{jtn}\sigma^I_{mn} \\ &\quad + \sum_{m,n=1}^{6} \varphi^E_{jsm}\varphi^E_{jtn}\sigma^E_{mn}\Bigg)\Bigg], \end{aligned} \tag{2}$$

where $f_j(\mathbf{q})$ is the atomic structure factor for atom j located at the average position $\langle\mathbf{r}_j\rangle$. In this formula, the Debye–Waller factor describing the dynamic structure of a protein is expanded in terms of normal modes of the enzyme. Subscripts I and E represent the internal and external normal modes, respectively. φ^I_{jsm} is the component of the mth normal mode obtained theoretically by normal-mode analysis, φ^E_{jsm} is that obtained by using the TLS model (Schomaker & Trueblood, 1968) and σ_{mn} is the covariance for the internal or external normal modes. The sum of the internal fluctuations is taken over the normal modes of the M lowest frequencies (the value of M to be determined below) and that of the external fluctuations is taken over six external modes. Therefore, after refinement, we can decompose the dynamic structure into the internal part representing shape-changing fluctuations of the enzyme and the external part caused by rigid-body fluctuations. Here, M is determined so as to balance the amount of experimental data with the number of parameters to be refined. This formula for the structure factor is based on the theoretical model of protein dynamics, which states that the conformational fluctuations of proteins can be described by a small number of low-frequency normal modes spanning the important conformational subspace (Go, 1990).

After the structure refinement with the isotropic thermal factors, the normal-mode refinement was performed in the following two stages. In the first stage, from the average coordinates obtained in the preceding refinement, the normal-mode vectors φ^I_{jsm} were computed after the energy-

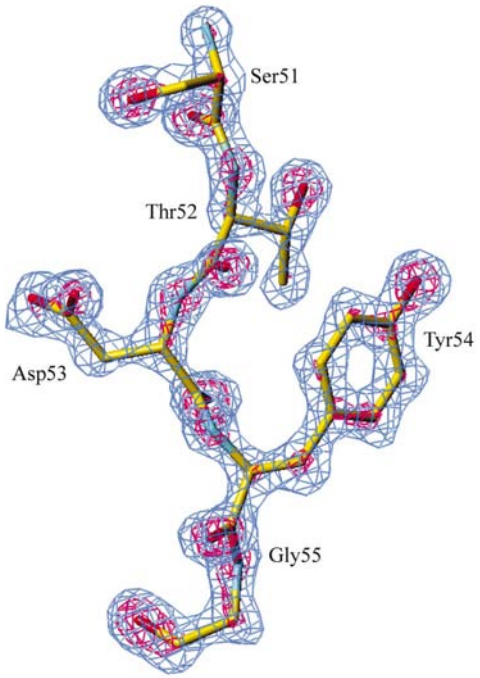

Figure 2
An omit-annealed $F_o - F_c$ map (coloured fishnet) for residues 51–55 (coloured stick model) of human lysozyme at 113 K. The map was calculated using reflections obtained between Bragg spacings of 8.0 and 1.4 Å and is contoured at a standard deviation level of 3.5σ (blue net) and 7.0σ (pink net).

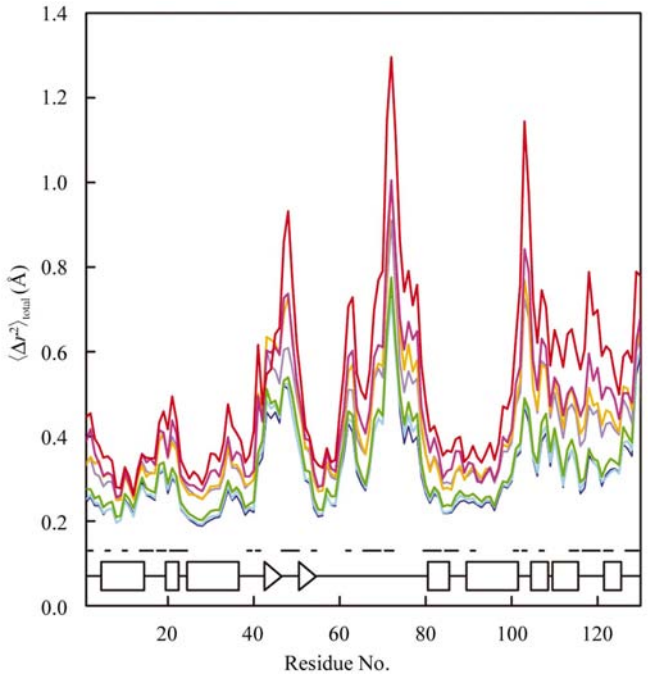

Figure 3
Temperature-dependent changes of mean-square fluctuations $\langle\Delta r^2\rangle_{\rm total}$ averaged for the main-chain atoms plotted against the residue number. They are measured at 113 (blue), 127 (cyan), 147 (green), 152 (purple), 161 (orange), 170 (pink) and 178 K (red). The lines inserted below the profiles indicate crystal-contact regions, in which the atoms of the residues are located within 3.8 Å from any atom of a symmetry-related molecule. A diagram of secondary structures in the enzyme is also shown, with boxes for α-helices and arrows for β-sheets.

minimization procedure using *PRESTO* (Morikami *et al.*, 1992) under the force-field parameters of *AMBER* (Weiner *et al.*, 1986). In the second stage, the average coordinates $\langle \mathbf{r}_j \rangle$ and the covariance σ_{mn} (2) were determined by crystallographic refinement minimizing the difference between the amplitudes of the calculated and observed structure factors. The model describing the structural fluctuations of human lysozyme is composed of the 100 lowest frequency normal modes for internal fluctuations and the six external modes for external fluctuations, with coupling among the 43 lowest frequency modes. In this model, the ratio between the number of observed reflections and that of the parameters refined ranged from 3.0 to 3.4. The fluctuations of solvent atoms are approximated by using isotropic thermal factors. A modified version of the program (Joti & Kidera, in preparation) was used to incorporate H atoms, generated in a rigid-body manner, and multiple occupancies for the side chains of Glu4, Glu7, Arg14, Leu25, Asn44 and Tyr63. The results of the normal-mode refinement are summarized in Table 1.

2.3. Anisotropic network model (ANM)

To clarify the effect of molecular packing on the dynamics of the enzyme, a simplified normal-mode analysis was carried out using an anisotropic network model (ANM; Atilgan *et al.*, 2001). This ANM model assumes that two residues within the cutoff distance of r_c are connected *via* a spring with force constant γ. Therefore, the potential energy of the system is

$$V = \frac{\gamma}{2} \sum_{r_{ij} < r_c} (r_{ij} - r_{ij}^X)^2, \tag{3}$$

where r_{ij} is the distance between residues i and j and superscript X denotes the X-ray structure. Here, we used a crystal structure refined at 113 K for r_{ij}^X. This immediately gives an estimation of mean-square fluctuations. The ANM analysis was carried out on a small system composed of eight unit cells (corresponding to 32 lysozyme molecules) under the conditions r_c = 9 Å, γ = 4.2 kJ mol^{-1} Å^{-2} and T = 300 K. The translational mean-square fluctuations of a whole molecule in the small crystal along the a axis, $\langle \Delta a_{\rm trans}^2 \rangle$, and the rotational mean-square fluctuations around the a axis, $\langle \Delta a_{\rm rot}^2 \rangle$, are calculated by

$$\langle \Delta a_{\rm trans}^2 \rangle = \left\langle \left| \frac{1}{N} \sum_{i=1}^{N} \Delta a_i \right|^2 \right\rangle = \frac{1}{N^2} \sum_m \frac{k_{\rm B} T}{\lambda_m} \sum_{i,j=1}^{N} v_{im}^a v_{jm}^a \tag{4}$$

and

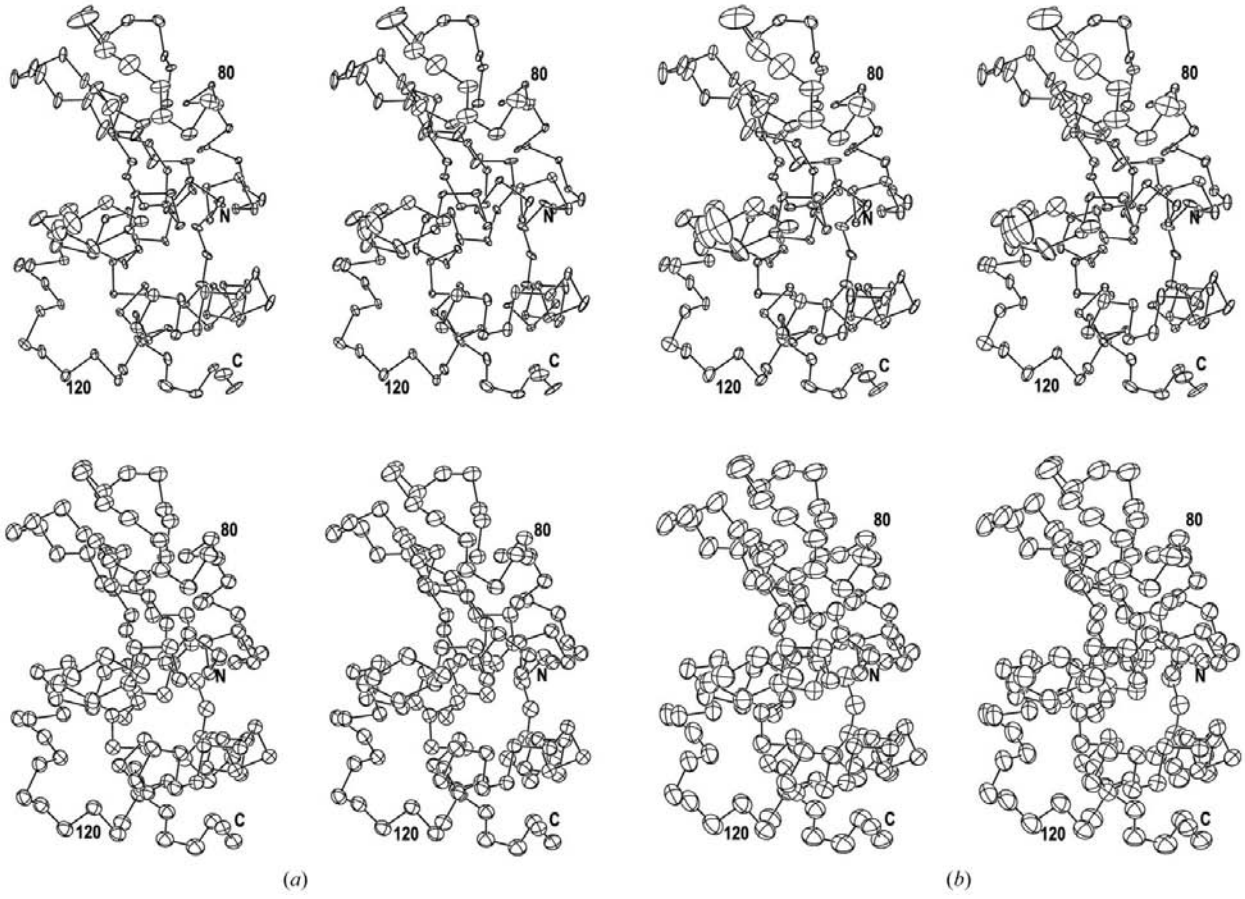

Figure 4
Stereo plots of $\langle \Delta r^2 \rangle_{\rm int}$ (top) and $\langle \Delta r^2 \rangle_{\rm ext}$ (bottom) mapped on the C$^\alpha$ trace using the *ORTEP* diagram (Burnett & Johnson, 1996). $\langle \Delta r^2 \rangle_{\rm int}$ and $\langle \Delta r^2 \rangle_{\rm ext}$ obtained at (*a*) 113 and (*b*) 170 K are shown as typical examples.

$$\langle \Delta a_{\rm rot}^2 \rangle = \frac{\omega_a^2}{N} \sum_i [(\mathbf{r}_i - \mathbf{r}_c) \times \mathbf{e}_a]^2, \quad (5)$$

with

$$\omega_a^2 = \left\langle \left\{ \mathbf{e}_a \cdot \mathbf{I}^{-1} \sum_i [(\mathbf{r}_i - \mathbf{r}_c) \times \Delta \mathbf{r}_i] \right\}^2 \right\rangle = \sum_m \frac{k_{\rm B} T}{\lambda_m} \sum_{i,j} [\mathbf{e}_a \cdot \mathbf{I}^{-1} (\mathbf{r}_i - \mathbf{r}_c) \times \mathbf{v}_{im}][\mathbf{e}_a \cdot \mathbf{I}^{-1} (\mathbf{r}_j - \mathbf{r}_c) \times \mathbf{v}_{jm}], \quad (6)$$

where N is the number of residues in the molecule, $\mathbf{r}_i$ and $\Delta\mathbf{r}_i$ are the coordinates and the positional fluctuation of atom i, respectively, Δa_i is the a-axis component of $\Delta\mathbf{r}_i$, $\mathbf{r}_c$ is the position vector of the center of mass, λ_m is the mth eigenvalue, $\mathbf{v}_{im}$ is the eigenvector for atom i and mode m, v_{im}^a is the a-axis component of $\mathbf{v}_{im}$, $\mathbf{e}_a$ is the unit vector representing the a axis, $\mathbf{I}$ is the inertia tensor of the molecule and $k_{\rm B}$ is the Boltzmann constant. The values of $\langle \Delta a_{\rm trans}^2 \rangle$ and $\langle \Delta a_{\rm rot}^2 \rangle$ for the molecule were calculated by averaging those values for four innermost molecules in the eight-cell crystal.

3. Results and discussion

3.1. Quality of the structural models and the ANM analysis

The seven sets of cryogenic diffraction data were collected successfully without any radiation damage to the crystal arising from long-term exposure to radiation from the laboratory X-ray source. In fact, neither the shape nor the height in the electron-density maps of the four S—S bonds in the enzyme changed (data not shown). The omit-annealed electron-density map (Fig. 2) had subatomic resolution, demonstrating the high quality of the diffraction data. The structural models after the normal-mode refinement had better crystallographic R factors than those obtained through ordinary refinement using *X-PLOR* and stereochemical parameters (Table 1). Fig. 3 shows the temperature-dependent variation in the mean-square fluctuations, $\langle \Delta r^2 \rangle_{\rm total}$, averaged for the main-chain atoms of each amino-acid residue. The normal-mode refinement separated the contributions from the internal $\langle \Delta r^2 \rangle_{\rm int}$ and external $\langle \Delta r^2 \rangle_{\rm ext}$ degrees of freedom to give the anisotropic thermal factors of the protein as shown in Fig. 4. The external degrees of freedom contribute more than 54% of the thermal factors and are more prominent at temperatures above 150 K, as described in the following sections.

The results of the theoretical ANM analysis of the small crystal system composed of eight cells are as follows. The magnitudes of the external fluctuations along the translational degrees of freedom are in the order $\langle \Delta c_{\rm trans}^2 \rangle$ (0.130 Å^2) > $\langle \Delta a_{\rm trans}^2 \rangle$ (0.080 Å^2) > $\langle \Delta b_{\rm trans}^2 \rangle$ (0.070 Å^2). In contrast, the external rotational fluctuations are in the order $\langle \Delta a_{\rm rot}^2 \rangle$ (0.057 Å^2) > $\langle \Delta b_{\rm rot}^2 \rangle$ (0.051 Å^2) > $\langle \Delta c_{\rm rot}^2 \rangle$ (0.039 Å^2). These orders of magnitudes correspond to the order of directions in which the enzyme in the crystal moves more easily, or in which it packs with other molecules more loosely. Therefore, the ANM analysis predicts that the enzyme is perturbed more along the c axis in the translational degrees of freedom and around the a axis in the rotational degrees of freedom.

3.2. Temperature dependence of dynamic structure

3.2.1. Transition-like behaviour of dynamic structure at around 150 K. Fig. 5(*a*) shows the temperature dependence of the mean-square fluctuations $\langle \Delta r^2 \rangle_{\rm total}$ and $\langle \Delta r^2 \rangle_{\rm int}$ averaged for the main-chain atoms and all non-H atoms. At temperatures below 150 K, $\langle \Delta r^2 \rangle_{\rm total}$ increases linearly with a small

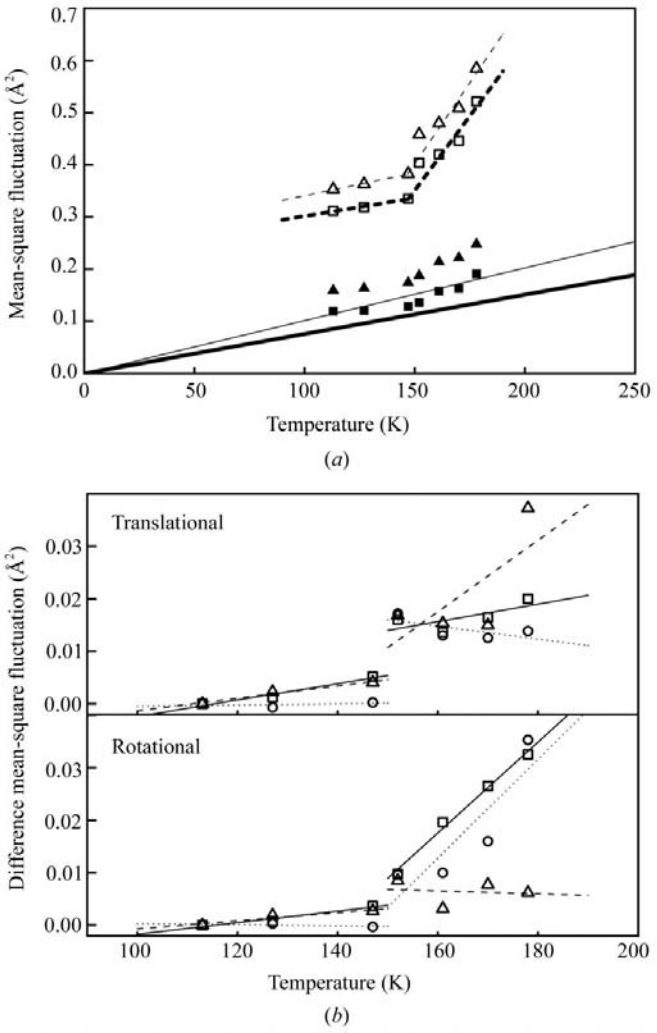

Figure 5
(*a*) Temperature dependence of mean-square fluctuations averaged for the main-chain atoms (squares) and for all non-H atoms (triangles). The total mean-square fluctuations $\langle \Delta r^2 \rangle_{\rm total}$ and the internal mean-square fluctuations $\langle \Delta r^2 \rangle_{\rm int}$ are shown by the open and filled symbols, respectively, together with best-fit lines (broken lines) calculated at temperatures below and above 150 K. Solid lines, thick for main-chain atoms and thin for all non-H atoms, show the temperature dependence of internal fluctuations predicted by theoretical normal-mode analysis. (*b*) The temperature dependence of external mean-square fluctuations $\langle \Delta r^2 \rangle_{\rm ext}$. Upper panel: translational components of $\langle \Delta r^2 \rangle_{\rm ext}$ along the a axis (square symbols), b axis (circles) and c axis (triangles) averaged for main-chain atoms are shown as the difference from the corresponding value at 113 K, together with regression lines (solid lines for the a axis, dotted lines for the b axis and broken lines for the c axis). Lower panel: the temperature dependence of rotational components around the three crystal axes shown using the same symbols.

gradient similar to that expected from the normal-mode analysis. In contrast, at temperatures above 150 K $\langle\Delta r^2\rangle_{\rm total}$ exhibits an obvious inflection. The gradient at temperatures above 150 K is significantly larger than in the normal-mode prediction. This sharp increase was not observed either in myoglobin (Chong *et al.*, 2001) or in RNase A (Rasmussen *et al.*, 1992; Tilton *et al.*, 1992). This temperature dependence is clearly the case in Fig. 1(*b*): when the crystal was heated to a temperature above 150 K, the molecule crossed potential barriers and found a new basin in the potential surface, which was not occupied at temperatures below 150 K. To understand the causes of the inflection, we analyzed $\langle\Delta r^2\rangle_{\rm int}$ and $\langle\Delta r^2\rangle_{\rm ext}$ separately, as will be described in the following sections.

3.2.2. Contribution from the external degrees of freedom. As shown in Fig. 5(*a*), the increase in fluctuations at above 150 K mainly originated from fluctuations arising from the external degrees of freedom $\langle\Delta r^2\rangle_{\rm ext}$. For further analyses, we decomposed $\langle\Delta r^2\rangle_{\rm ext}$ into several components. Since the off-diagonal elements of the variance–covariance matrix of the external variables have magnitude almost one order smaller than those of the diagonal elements, the six diagonal components, the three translational and the three rotational variances, are sufficient to explain the characteristics of the external fluctuations. As shown in Fig. 5(*b*), at temperatures above 150 K the magnitudes of the translational fluctuations are in the order $\langle\Delta c^2_{\rm trans}\rangle > \langle\Delta a^2_{\rm trans}\rangle > \langle\Delta b^2_{\rm trans}\rangle$. In contrast, the magnitudes of the rotational fluctuations are in the order $\langle\Delta a^2_{\rm rot}\rangle > \langle\Delta b^2_{\rm rot}\rangle > \langle\Delta c^2_{\rm rot}\rangle$. These orders of magnitudes agree well with those predicted by the ANM analysis (§3.1), suggesting that an increase in fluctuations at above 150 K occurs in the direction in which the enzyme molecules are less tightly packed or have weak contacts.

3.2.3. Contribution from the internal degrees of freedom. At temperatures below 150 K, the fluctuations arising from the internal degrees of freedom $\langle\Delta r^2\rangle_{\rm int}$ show a temperature dependence basically similar to that of crystalline myoglobin (Chong *et al.*, 2001), which can be approximated as $\langle\Delta r^2\rangle_{\rm int} = \alpha T + \beta$, where α is the gradient predicted by the normal-mode analysis and β reflects the distribution of conformational substates at 0 K. Because of the inflection at temperatures beyond 150 K, we estimated the incremental gradient in $\langle\Delta r^2\rangle_{\rm int}$ contributing to the inflection in each amino-acid residue using

$$D_i = |\alpha_i^{\rm high} - \alpha_i^{\rm low}|, \qquad (7)$$

where $\alpha_i^{\rm low}$ is the gradient of the linear-regression line calculated using the internal fluctuations of the ith residue, $\langle\Delta r_i^2\rangle_{\rm int}$, averaged for three data sets obtained at temperatures below 150 K and $\alpha_i^{\rm high}$ is that for the other four data sets obtained at temperatures above 150 K. The values of D_i were compared with the values of $\langle\Delta r_i^2\rangle_{\rm int}$ obtained at 113 K (Fig. 6). All the values are similar; the correlation coefficient between the profiles is 0.66. Therefore, we believe that the increase in the internal fluctuations at temperatures above ~150 K occurred in the residues with inherently high flexibility. This is consistent with the results of the analyses of fluctuations arising from

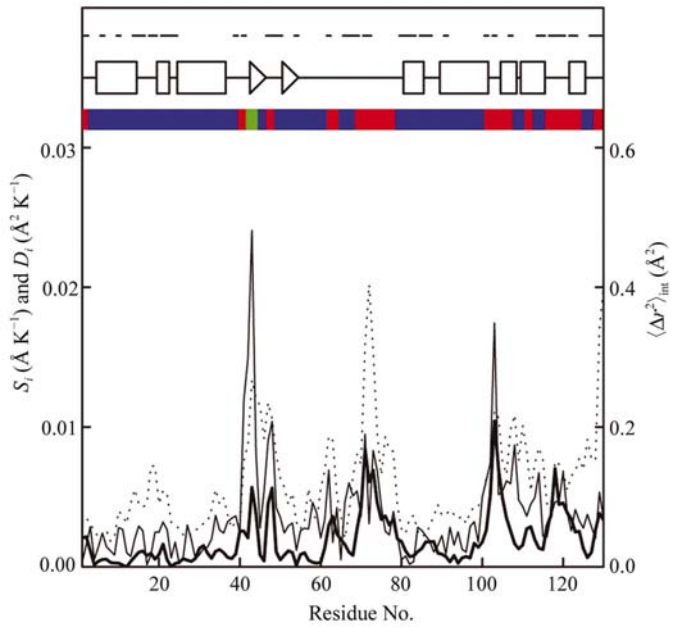

Figure 6
The values of D_i (thick solid curve) calculated using (7), those of S_i (thin solid curve) calculated using (9) and those of $\langle\Delta r^2\rangle_{\rm int}$ at 113 K (dotted curve) are plotted against the residue number. The diagrams for crystal-contact regions and secondary structures are shown in the inset as in Fig. 3. The upper coloured boxes indicate three types of dynamic response: 'harmonic' (blue), 'glassy' (red) and 'shifted' (green).

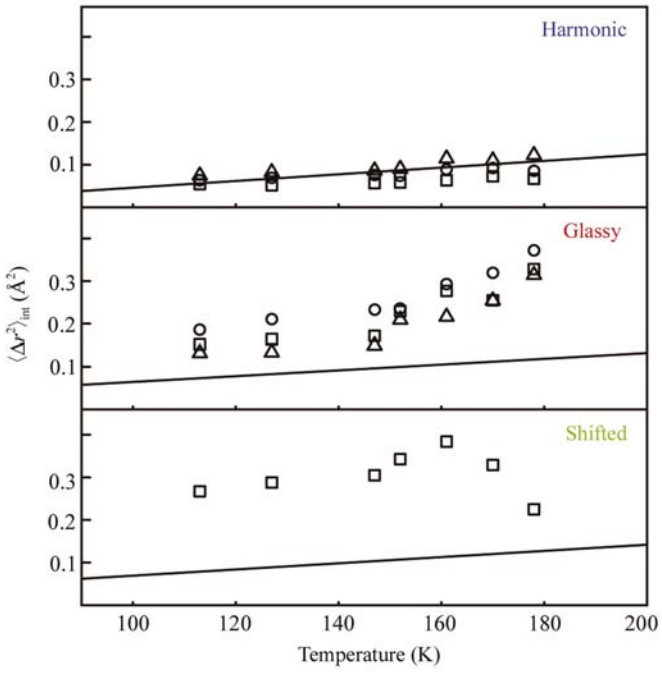

Figure 7
Typical examples of the three types of dynamic response based on the temperature dependence of internal fluctuations: Leu25 (square), Tyr54 (circle) and Asp91 (triangle) representing the residues with 'harmonic' responses, Arg41 (square), Ala76 (circle) and Ile106 (triangle) showing 'glassy' responses and Thr43 (square) showing 'shifted' responses. The solid lines show the temperature dependence of $\langle\Delta r^2\rangle_{\rm int}$ predicted by theoretical normal-mode analysis for Leu25, Arg4 and Thr43.

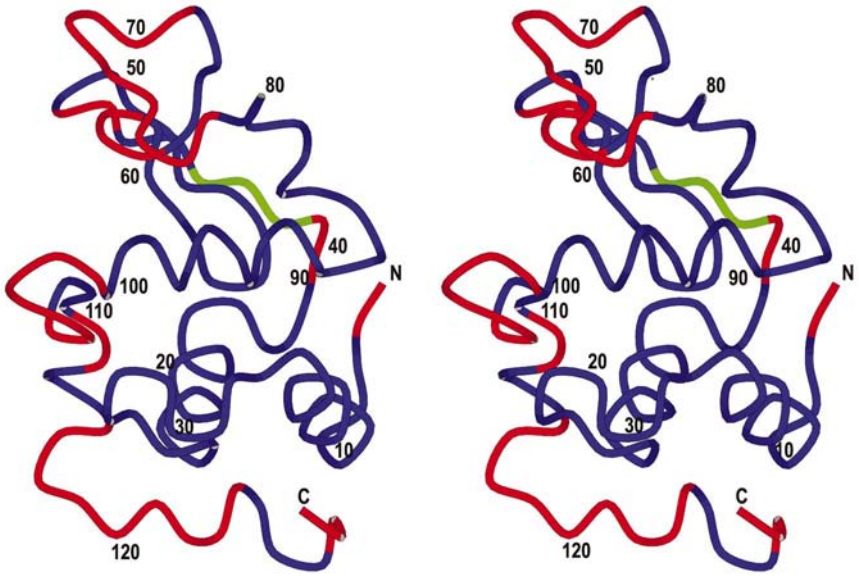

Figure 8
A stereo plot mapping the three types of dynamic response of internal fluctuations onto the C^{α} trace of the enzyme structure. The colouring scheme is the same as in Fig. 6. The drawing was generated by *MOLSCRIPT* (Kraulis, 1991).

the external degrees of freedom, in which large responses were observed in the directions in which the enzymes were less packed or had weak contacts.

Based on the temperature dependence of $\langle \Delta r_i^2 \rangle_{\rm int}$, we classified the dynamic responses of the residues into three groups as described in Fig. 1. In the residues with the dynamic responses termed as 'harmonic', the internal mean-square fluctuations increase linearly throughout the temperature range (Fig. 1*a*). The residues whose value of $\langle \Delta r_i^2 \rangle_{\rm int}$ shows a single upward inflection at ~150 K were classified as 'glassy' (Fig. 1*b*). In the residues with the dynamic response termed as 'shifted', $\langle \Delta r_i^2 \rangle_{\rm int}$ first rises at ~150 K but then decreases at a higher temperature (Fig. 1*c*). We found that 40 residues exhibit the 'glassy' response and three residues show the 'shifted' response; the remaining 87 residues were classified as 'harmonic'. The

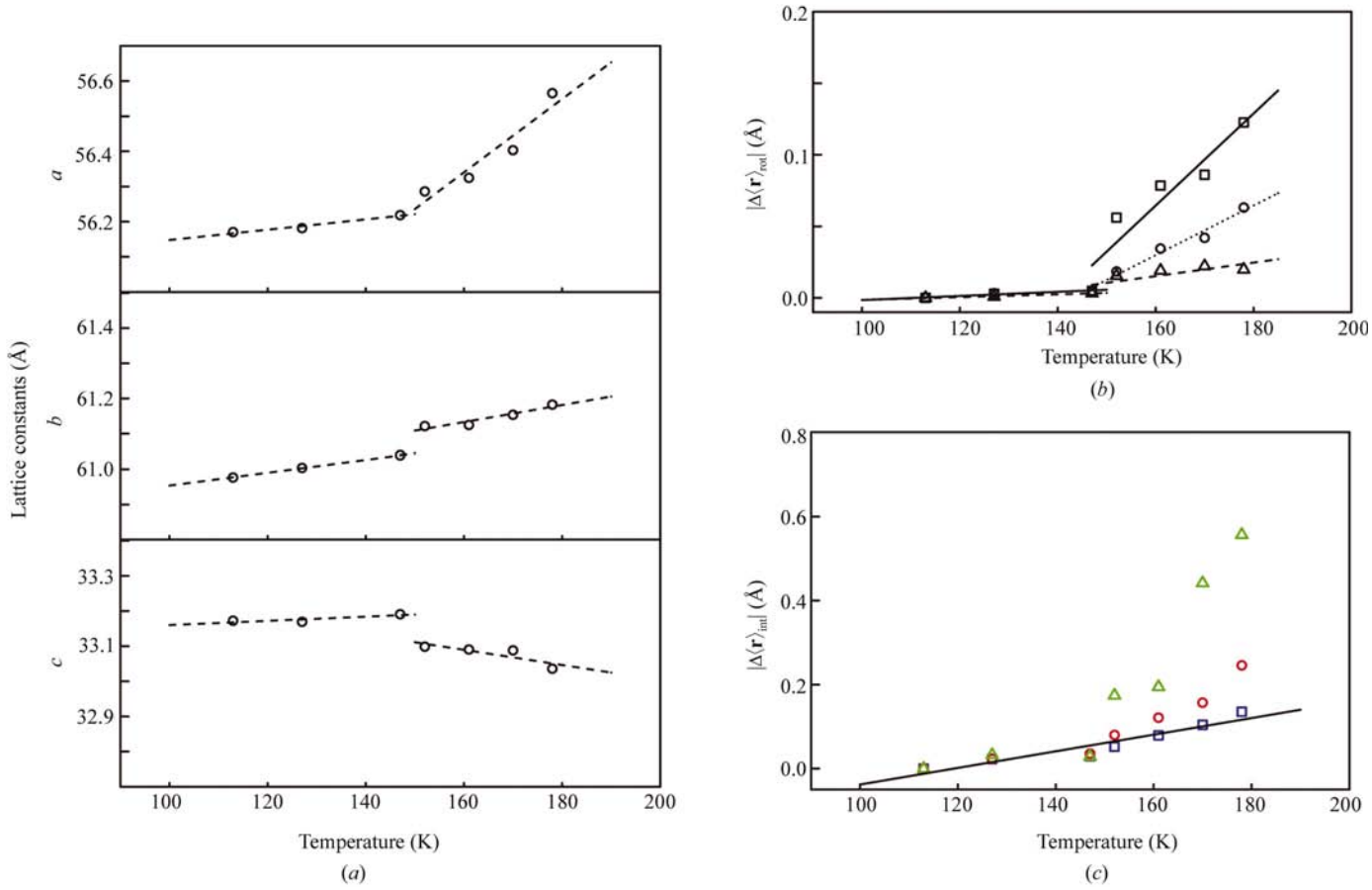

Figure 9
(*a*) Temperature dependence of lattice constants. (*b*) Temperature dependence of $|\Delta\langle \mathbf{r} \rangle_{\rm rot}|$ averaged for main-chain atoms. The symbols and lines are the same as in Fig. 5(*b*). (*c*) Temperature dependence of $|\Delta\langle \mathbf{r} \rangle_{\rm int}|$ averaged for the residues with each type of dynamic response; the colouring scheme is the same as in Fig. 6. A linear regression line is drawn only for the 'harmonic' class.

threshold value of D_i distinguishing the harmonic and glassy (or shifted) residues was 0.002 Å^2 K^{-1}. The three residues with 'shifted' responses show a marked decrease in the values of $\langle\Delta r_i^2\rangle_{\rm int}$ at ∼160 K and negative values of $\alpha_i^{\rm high} - \alpha_i^{\rm low}$. Some typical examples of the three groups of residues are shown in Fig. 7. Fig. 8 maps the dynamic responses of the residues on the crystal structure of the enzyme. It is clear that the residues with 'glassy' responses were mostly found in the flexible part exposed to the solvent and in the loop region, particularly at the edges of the two lobes forming the cleft of the enzyme.

In the residues with 'harmonic' responses, the distributions of conformational substates do not change when the temperature exceeds 150 K (Fig. 1*a*). In contrast, in the residues with 'glassy' responses, the substates not occupied at temperatures below 150 K become occupied at higher temperatures (Fig. 1*b*). In the residues with 'shifted' response, the dynamic response is 'glassy' at ∼150 K, but then large coordinate shifts occur at ∼160 K, which change the distribution of conformational substates so that the substates occupied at temperatures below 150 K disappear (Fig. 1*c*). Such coordinate shifts result in a decrease in $\langle\Delta r_i^2\rangle_{\rm int}$, as seen in Fig. 7. In the residues of this type, a decrease in the Debye–Waller factor may also be detected by an incoherent experiment, although conducting such a site-specific experiment may not be so easy (Zaccai, 2000). This pattern of dynamic response was found only in residues 42–44. These three residues show anomalies also in their static structure, as will be discussed in the following section.

3.3. Temperature dependence of static average structure and correlation with that of dynamic structure

To analyze the dependence of the static structure on temperature, the displacement $\Delta\langle\mathbf{r}\rangle$ of the average position at two different temperatures was divided into three components using

$$\Delta\langle\mathbf{r}\rangle = \Delta\langle\mathbf{r}\rangle_{\rm trans} + \Delta\langle\mathbf{r}\rangle_{\rm rot} + \Delta\langle\mathbf{r}\rangle_{\rm int}, \qquad (8)$$

where $\Delta\langle\mathbf{r}\rangle_{\rm trans}$ is the translational displacement of the centre of gravity of the molecule, $\Delta\langle\mathbf{r}\rangle_{\rm rot}$ is the rotational displacement and $\Delta\langle\mathbf{r}\rangle_{\rm int}$ is the internal displacement.

3.3.1. Temperature dependence of the translational component. The quantity $\Delta\langle\mathbf{r}\rangle_{\rm trans}$ corresponds to the temperature-dependent changes in the lattice constants (Fig. 9*a*). One can see in the figure an apparent inflection in the temperature dependence of the lattice constant a at ∼150 K, concomitant with the inflection in the temperature dependence of $\langle\Delta r^2\rangle_{\rm total}$. Lattice constants b and c change almost linearly, but appear to have small abrupt jumps at ∼150 K: the cell slightly expands along the b axis and shrinks along the c axis at temperatures above 150 K.

3.3.2. Temperature dependence of the rotational component. Fig. 9(*b*) shows that the values of $|\Delta\langle\mathbf{r}\rangle_{\rm rot}|$ around the a and the b axes show inflections at ∼150 K and increase linearly at temperatures above 150 K. The value around the a axis is about two times greater than that around the b axis. In contrast, $|\Delta\langle\mathbf{r}\rangle_{\rm rot}|$ around the c axis is vanishingly small throughout the whole temperature range. Here, it is noticed that there is a strong correlation between the obtained rotational component in $\langle\Delta r^2\rangle_{\rm ext}$ (Fig. 5*b*), $|\Delta\langle\mathbf{r}\rangle_{\rm rot}|$ (Fig. 9*b*) and the results of the ANM analysis (§3.1). From this strong correlation, we conclude that the response of $\Delta\langle\mathbf{r}\rangle_{\rm rot}$ at 150 K occurs in the direction in which the enzyme molecules are less tightly packed or have weak contacts.

3.3.3. Temperature dependence of the internal component. Fig. 9(*c*) shows the temperature dependence of $|\Delta\langle\mathbf{r}\rangle_{\rm int}|$ averaged for the residues with dynamic responses of each group. The values for the residues with the 'harmonic' responses clearly show almost linear temperature dependence. The values for the residue with the 'glassy' responses show an inflection at ∼150 K, while those for the residue with 'shifted' responses exhibit the largest coordinate shifts at temperatures above ∼150 K, as illustrated in Figs. 1(*b*) and 1(*c*).

As in (7), we estimated the incremental gradient in $|\Delta\langle\mathbf{r}\rangle_{\rm int}|$ contributing to the inflection in each amino-acid residue by

$$S_i = |\gamma_i^{\rm high} - \gamma_i^{\rm low}|, \qquad (9)$$

where $\gamma_i^{\rm low}$ and $\gamma_i^{\rm high}$ are the gradients of linear-regression lines calculated in a manner similar to that in (7). The values of S_i are plotted in Fig. 6 and are in good agreement with the values of D_i representing the dynamic response (correlation coefficient of 0.62). From Fig. 6, the residues exhibiting 'glassy' responses have a large increase in $|\Delta\langle\mathbf{r}\rangle_{\rm int}|$ above

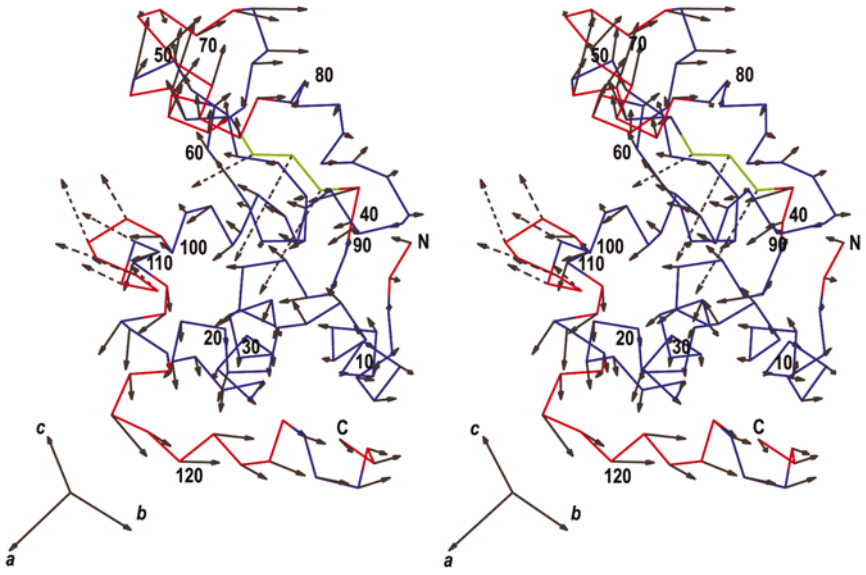

Figure 10
A stereo plot of the difference, $\Delta\langle\mathbf{r}\rangle_{\rm int}$, between the coordinates at 113 K and those at 178 K. $\Delta\langle\mathbf{r}\rangle_{\rm int}$ is shown by the arrows (magnified 15 times for easy perception) mapped onto the C$^\alpha$ trace of lysozyme. The anomalous behaviour of $\Delta\langle\mathbf{r}\rangle_{\rm int}$ for residues 42–44 and 102–108 is highlighted by the broken arrows. The drawing was generated by *MOLSCRIPT* (Kraulis, 1991).

the transition temperature. This situation is illustrated in Fig. 1(*b*). The average value of S_i for the residues with 'glassy' responses is about two times greater than that for the residue with 'harmonic' responses: $\langle S_i \rangle_{\rm glassy} = 5.2 \times 10^{-3}$ Å K^{-1} and $\langle S_i \rangle_{\rm harmonic} = 2.5 \times 10^{-3}$ Å K^{-1}. The S_i values of residues 42–44 are remarkably large ($\langle S_i \rangle_{\rm shifted} = 1.6 \times 10^{-2}$ Å K^{-1}), probably because of the inherent structural disorder of the region of residues 42–44. In fact, when evaluating the average root-mean-square deviation for all crystal structures of human lysozyme in the PDB (148 entries), we found remarkably large values (about 0.7 Å) in these residues, compared with the average value of about 0.2 Å for all other residues. The large values of S_i in residue 106 appear to be a result of the anomalies in residues 42–44, because residue 106 forms hydrogen bonds with residues 42–44 of a symmetry-related molecule *via* a few well defined water molecules.

In Fig. 10, the direction and magnitude of $\Delta\langle \mathbf{r} \rangle_{\rm int}$ in each residue are mapped on the crystal structure. Except in residues 42–44 and 102–108, the coherent pattern of $\Delta\langle \mathbf{r} \rangle_{\rm int}$ shown by the arrows appears to indicate the opening and closing of the active-site cleft. This pattern is actually very similar to that of the eigenvectors of the two lowest frequency modes (3.72 and 5.29 cm^{-1}) found in the normal-mode analysis of the enzyme (Gibrat & Go, 1990). This observation leads us to conclude that the response of the static average structure occurs in the mode with the largest fluctuations, or in the lowest frequency modes.

In summary, the experimental results and theoretical calculations described above indicate that the perturbation occurring at the transition temperature causes a shift of the static average coordinates in the direction of larger fluctuations. At the same time, the dynamic fluctuations in the same direction are enhanced.

3.4. Possible causes for changes in both the dynamic and static structures at around 150 K

As described above, based on the temperature dependence of internal fluctuations, the dynamic responses can be classified into three types, namely, 'harmonic', 'glassy' and 'shifted' (Fig. 7). In Fig. 11, the distribution of responses of these three types is mapped onto the crystal lattice viewed down the *c* axis. The residues with 'glassy' and 'shifted' responses are localized mainly in the region facing a large solvent channel running through the crystal parallel to the *c* axis. Such an anomaly of the solvent channel was also observed in the solvent structure. The decrease in the number of water molecules at temperatures above 150 K shown in Table 1 occurs mostly in the surface area exposed to the solvent channel (data not shown).

Because cubic ice starts to form in water at around 150 K (Mishima & Stanley, 1998), we consider that the transition-like behaviour of the dynamic and static structures of the enzyme may have been enhanced by the early stage of cubic ice formation in the solvent channel. In fact, in the diffraction patterns obtained at temperatures above 150 K, we observed weak Debye–Scherrer patterns that we thought to arise from cubic ice formation (data not shown). Because a small amount of mother liquor remained around the crystal, it is difficult to judge whether the diffraction patterns came from inside or outside the crystal. However, it is plausible that the cubic ice formation in the solvent channel expanded the cell size and subsequently induced a shift of the static coordinates and an increase in the fluctuations. This conjecture is supported by a report that similar cell expansion occurred in various protein crystals having large solvent channels and that the magnitude of expansion correlates with the size of solvent channels (Weik *et al.*, 2001). In addition, neither glass-to-cubic transition nor cubic-to-hexagonal transition occurred in a rubredoxin crystal having a very small number of water molecules (Nakasako, unpublished results). This can also explain why such a transition was not observed in myoglobin (Chong *et al.*, 2001). Comparing the crystal structure of lysozyme and that of myoglobin (Figs. 12*b* and 12*c*), we notice that the myoglobin crystal does not have an apparent solvent channel. Therefore, the size of solvent channels may be the most plausible explanation for the difference in the temperature dependence of the static and dynamic structures between the lysozyme and myoglobin crystals.

The analysis in this work indicates that the transition at 150 K may be caused by cubic ice formation in the large solvent

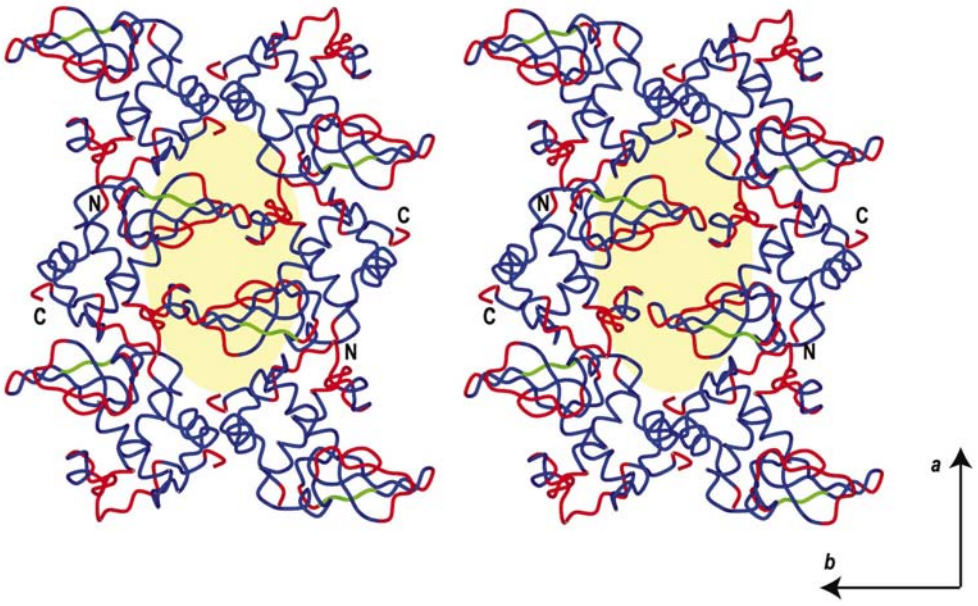

Figure 11
(*a*) A stereo plot mapping the dynamic responses of the residues in the crystal lattice. Six molecules along the *ab* plane are shown. Polypeptide chains are coloured as in Fig. 8. The solvent channel along the *c* axis is indicated by the yellow ellipse.

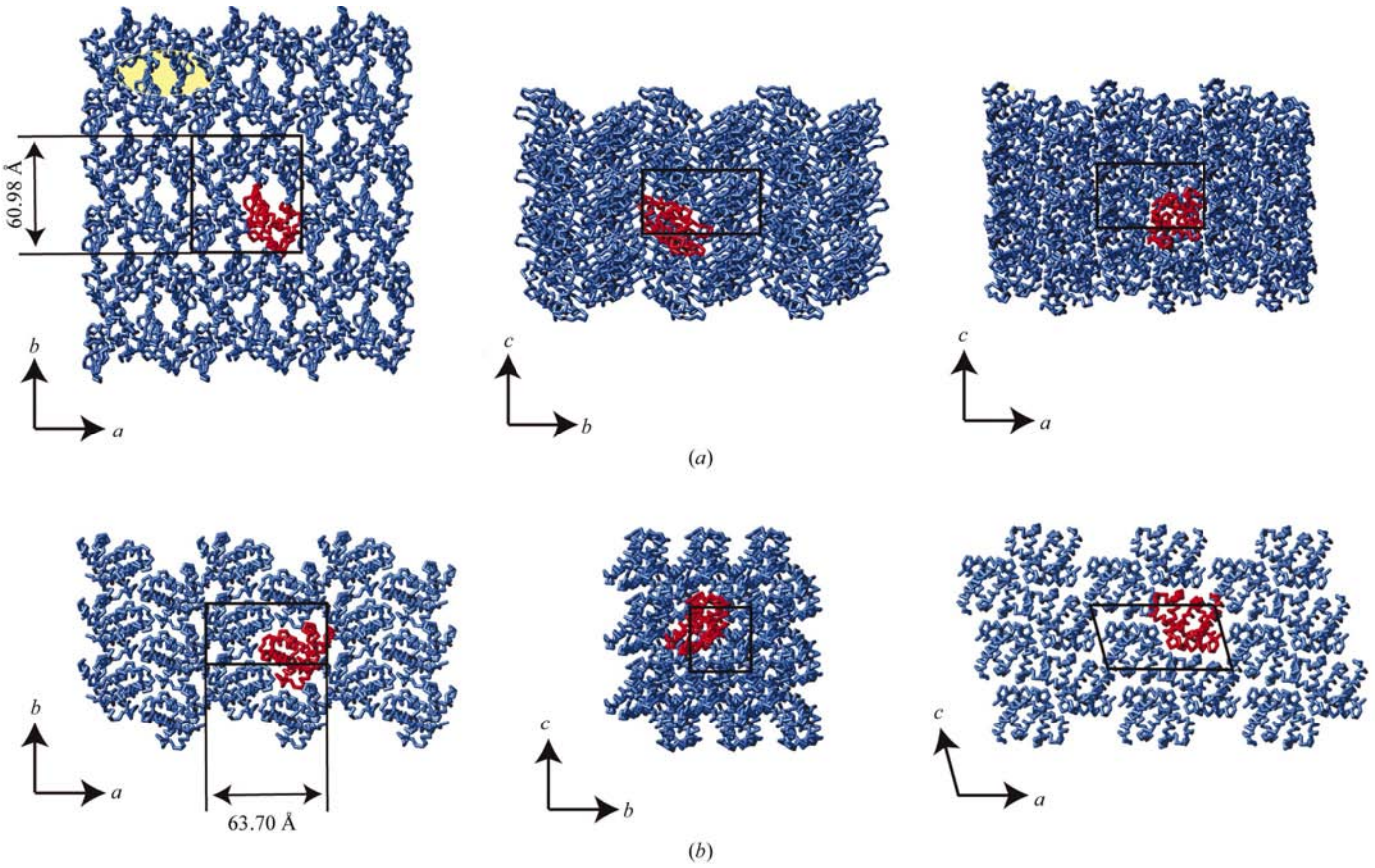

Figure 12
(*a*) The arrangement of human lysozyme molecules in the orthorhombic crystal. Views from three directions along the crystal axes are shown and the molecules are presented as C^{α} traces. For clarity, a molecule occupying a crystallographic asymmetric unit is shown in red. The yellow ellipse in the *ab* plane is the same as in Fig. 11. The box indicates the unit cell. (*b*) The arrangement of myoglobin molecules in the monoclinic crystal used in our previous study (Chong *et al.*, 2001). The three panels are drawn in the same way as in (*a*).

channels of the crystal. Similarly, Daniel *et al.* (1999) recently observed dynamic transition at ∼150 K in the incoherent inelastic neutron scattering of *a hydrated powder sample* of glutamate dehydrogenase. This suggests that the transition observed in the lysozyme crystal occurs also in hydrated powder.

Finally, we point out the history-dependent behaviour of the crystal we studied in this work. As described in §2.1, the crystal grown at the room temperature was flash-cooled to 113 K and measurements were performed heating it gradually to 178 K. Even though no measurement was performed on this crystal before flash-cooling, the value of $\langle \Delta r^2 \rangle_{\rm total}$ observed previously for another crystal of the same molecule at 282 K was 0.49 Å^2 (Kidera *et al.*, 1992). This value is comparable to the value 0.52 Å^2 obtained in this study at 178 K (Fig. 5*a*) and would have become even larger if measurements could be continued at higher temperatures. Therefore, it is concluded that the crystal structure after flash-cooling is in a metastable state depending on its history.

The authors would like to thank Professor K. Yutani and Dr K. Takano of Osaka University for their preparation of the human lysozyme solution sample. This work was supported by a grant from the MEXT to MN, AK and NG. The computations were performed at the Computer Center of the Institute for Molecular Science, the Center for Promotion of Computer Science and Engineering of JAERI.

References

Atilgan, A. R., Durell, S. R., Jernigan, R. L., Demirel, M. C., Keskin, O. & Bahar, I. (2001). *Biophys. J.* **80**, 505–515.
Berman, H. M., Westbrook, J., Feng, Z., Gilliland, G., Bhat, T. N., Weissig, H., Shindyalov, I. N. & Bourne, P. E. (2000). *Nucleic Acids Res.* **28**, 235–42.
Brünger, A. T. (1992). *X-PLOR Version 3.1: A System For X-ray Crystallography and NMR.* Yale University, Connecticut, USA.
Burnett, M. N. & Johnson, C. K. (1996). *ORTEP-III: Oak Ridge Thermal Ellipsoid Plot Program For Crystal Structure Illustrations.* Report ORNL-6895, Oak Ridge National Laboratory, Tennessee, USA.
Chong, S.-H., Joti, Y., Kidera, A., Go, N., Ostermann, A., Gassmann, A. & Parak, F. (2001). *Eur. Biophys. J.* **30**, 319–329.
Daniel, R. M., Finney, J., Réat, V., Dunn, R., Ferrand, M. & Smith, J. C. (1999). *Biophys. J.* **77**, 2184–2190.
Doster, W., Cusack, S. & Petry, W. (1989). *Nature (London)*, **337**, 754–756.
Engh, R. A. & Huber, R. (1991). *Acta Cryst.* A**47**, 392–400.

Ferrand, M., Dianoux, A. J., Petry, W. & Zaccai, G. (1993). *Proc. Natl Acad. Sci. USA*, **90**, 9668–9672.
Frauenfelder, H. (1989). *Int. J. Quantum Chem.* **35**, 711–715.
Frauenfelder, H., Petsko, G. A. & Tsernoglou, D. (1979). *Nature (London)*, **280**, 558–563.
Gibrat, J.-F. & Go, N. (1990). *Proteins*, **8**, 258–279.
Go, N. (1990). *Biophys. Chem.* **35**, 105–112.
Hagen, S. J., Hofrichter, J. & Eaton, W. A. (1995). *Science*, **269**, 959–962.
Hartmann, H., Parak, F., Steigemann, W., Petsko, G. A., Ponzi, D. R. & Frauenfelder, H. (1982). *Proc. Natl Acad. Sci. USA*, **79**, 4967–4971.
Kidera, A. & Go, N. (1992). *J. Mol. Biol.* **225**, 457–475.
Kidera, A., Inaka, K., Matsushima, M. & Go, N. (1992). *J. Mol. Biol.* **225**, 477–486.
Kraulis, P. J. (1991). *J. Appl. Cryst.* **24**, 946–950.
Kurinov, I. V. & Harrison, R. W. (1995). *Acta Cryst.* D**51**, 98–109.
Mishima, A. & Stanley, H. E. (1998). *Nature (London)*, **396**, 329–355.
Morikami, K., Nakai, T., Kidera, A., Saito, M. & Nakamura, H. (1992). *Comput. Chem.* **16**, 243–248.
Muraki, M., Harata, K., Sugita, N. & Sato, K. (1996). *Biochemistry*, **35**, 13562–13567.
Nagata, C., Moriyama, H., Tanaka, N., Nakasako, M., Yamamoto, M., Ueki, T. & Oshima, T. (1996). *Acta Cryst.* D**52**, 623–630.
Nakasako, M. (2001). *Cell. Mol. Biol.* **47**, 767–790.
Nienhaus, G. U. & Parak, F. (1986). *Hyperfine Interact.* **29**, 1451–1454.
Otwinowski, Z. & Minor, W. (1997). *Methods Enzymol.* **276**, 307–326.
Parak, F., Hartmann, H., Aumann, K. D., Reuscher, H., Rennekamp, G., Bartunik, H. & Steigemann, W. (1987). *Eur. Biophys. J.* **15**, 237–249.
Parak, F., Knapp, E. W. & Kucheida, D. (1982). *J. Mol. Biol.* **161**, 177–194.
Rasmussen, B. F., Stock, A. M., Ringe, D. & Petsko, G. A. (1992). *Nature (London)*, **357**, 423–424.
Schomaker, V. & Trueblood, K. N. (1968). *Acta Cryst.* B**24**, 63–76.
Takano, K., Ogasahara, K., Kaneda, H., Yamagata, Y., Fujii, S., Kanaya, E., Kikuchi, M., Oobatake, M. & Yutani, K. (1995). *J. Mol. Biol.* **254**, 62–76.
Tilton, F., Dewan, J. C. & Petsko, G. A. (1992). *Biochemistry*, **31**, 2469–2481.
Weik, M., Kryger, G., Schreurs, A. M. M., Bouma, B., Silman, I., Sussman, J. L., Gros, P. & Kroon, J. (2001). *Acta Cryst.* D**57**, 566–573.
Weiner, S. J., Kollman, P. A., Nguyen, D. T. & Case, D. A. (1986). *J. Comput. Chem.* **7**, 230–252.
Zaccai, G. (2000). *Science*, **208**, 1604–1607.